Bull. Nov. Comp. Center, Num. Model. in Atmosph., etc., 7 (2001), 1–16

On the numerical modeling of the World Ocean circulation in the sigma coordinate system*

E.N. Goloubeva

The World Ocean Circulation Model based on the σ-coordinate transformation was modified to improve the pressure gradient force approximation and the diffusion transport presentation. The model was integrated for 1000 years to reproduce the general circulation and the thermohaline distribution for the World ocean.

1. Introduction

The terrain following the σ-coordinate system is one of approaches used in the ocean dynamic modeling for treatment of the vertical coordinate. Among the ocean numerical models employing the σ-coordinate system are the Princeton Ocean Model [1], and the Spectral Primitive Equation Model [2], which are usually used for research into the limited regions. Starting in the 80s, two russian σ-coordinate models were developed for the climate study in the World Ocean basin [3–8].

Numerical ocean models, employing the σ-coordinate transformation, have at least two main problems to be solved, namely, to make the correct approximation for the horizontal pressure gradients and to realistically describe the diffusion transport processes. Since the 70-s the question about errors in computing the pressure gradient force in the numerical weather prediction models employing the σ-coordinate system was brought to attention of the ocean modellers. The estimates for these errors depending on topography, stratification and grid spacing were represented in [9] and [10]. There have been many attempts to improve the situation and to reduce the pressure gradient errors. A number of methods have been proposed, namely: subtracting a mean vertical density before computing the pressure gradients, implementing a high-order discretization of the pressure gradient term, calculating the pressure gradient on the basis of the z-coordinate approach. The references to these approaches can be found in [11]. The question about the energy and momentum consistency for different pressure gradient approximations in the σ-coordinate system was investigated in [12].

*Supported by ARC Small Grant-1999 and by the Leading Scientific Schools Grant 00-15-98543.

The second important question is an accurate calculation of the diffusive transport processes. For us this problem was firstly detected when the World Ocean Circulation Model (hereafter the WOCM) based on the σ-coordinate transformation was developed in the Laboratory of Oceanography of the Computing Center of the Siberian Branch, Russian Academy of Sciences in the 80s [3–5]. In 1985, Mellor and Blumberg [13] wrote that the full transformation formula for the diffusive transport terms brought about serious errors on the sloping bottoms and proposed an approximate formula by neglecting the cross-derivative terms in the transformed diffusive operator. Most of the numerical modeling experiments, based on the σ-coordinate models, employ this approximation. The neglection of the cross-derivative terms could not improve the situation as it resulted in the spurious diffusion depending on the model topography and generated the topography-dependent thermocline distribution followed by considerable errors in the deep layer ocean circulation. The work by Huang and Spaulding [14], represents a new formula for the horizontal diffusion to provide a realistic calculation, but the numerical test for only 30 days of integration is provided as a proof of the problem solution. In 1998, Moshonkin et al. [7] used a new representation of the horizontal heat and salt exchange in their World Ocean σ-coordinate model [6–8], which corresponds to the exact transformation formula. The authors wrote that including the cross-derivative terms for the calculation of the horizontal turbulent heat and salt exchange leads to a decrease in temperature in the deep oceanic layers, approaching the real distributions.

Starting with the first goal of comparison between the ocean models employed different numerical techniques for the treatment of the vertical coordinate, namely, the horizontal z-levels, reducing the observed topography to a series of steps, and the σ-coordinate system, we had to make some changes in the main σ-model code [3–5], connected with the solution of the previously described problems. For the first problem solution we used the z-coordinate based on pressure gradient calculation. When dealing with the diffusion transport problem, an unexpected idea based on the contrast with the previously used method [15] helped to obtain an appropriate solution. These improvements enables us to run the long-period integration on the basis of the sigma-coordinate World Ocean circulation model and to make a comparison with the same results for the z-level based model [16]. In this paper, we just focus on the main numerical peculiarities in the ocean modeling based on the σ-coordinate system.

2. The σ-coordinate approach and its problems

The topography-following σ-coordinate system widely used in the oceanographic community was first introduced by Phillips [17], for the numeri-

cal modeling in weather prediction. With the framework of this approach, the Cartezian coordinates (x, y, z) are transformed to the sigma coordinates (x, y, σ) by

$$x_* = x, \quad y_* = y, \quad \sigma = \frac{z}{H(x,y)}, \tag{1}$$

where $H(x, y)$ is the bottom topography. The new vertical coordinate σ increases from $\sigma = 0$ at the sea surface to the $\sigma = 1$ at the ocean bottom for any oceanic point, and when applied the vertical grid has now the same number of points for any water column independent of the water depth. The mathematical equation model formulated in the σ-coordinate system have some disadvantages which should be overcome to have reliable results of numerical modeling.

2.1. Pressure gradient approximation. The first of the most significant disadvantages of models based on the σ-coordinate transformation is poor approximation of the horizontal gradients in the vicinity of the steep topography slopes. According to the vertical coordinate transformation the horizontal pressure gradient in the new coordinates can be expressed as:

$$\frac{\delta p}{\delta x} = \frac{\delta p}{\delta x_*} - \frac{\sigma}{H}\frac{\delta H}{\delta x_*}\frac{\delta p}{\delta \sigma}. \tag{2}$$

The use of this equation corresponds to evaluating a small term $\frac{\delta p}{\delta x}$ as subtraction of the two large ones $\frac{\delta p}{\delta x_*}$ and $\frac{\sigma}{H}\frac{\delta H}{\delta x_*}\frac{\delta p}{\delta \sigma}$. Caused by inessential truncation errors in these two terms approximation, serious errors can occur in the pressure gradient followed by artificial flows in numerical results, especially in the vicinity of a steep slope, where the grid cells are vertically stretched. It is the so-called "hydrostatic inconsistency" [18, 9]. In fact, if we want a grid to be "hydrostatically consistent", then we have to set the spatial discretization according to the following constraint:

$$\frac{\Delta x}{H}\frac{\delta H}{\delta x} \leq \frac{\Delta \sigma}{\sigma}, \tag{3}$$

where Δx and $\Delta \sigma$ are the grid sizes in the horizontal and the vertical directions, respectively. This condition requires a high horizontal resolution near the steep bottom slopes, or it restricts the inclusion of the realistic bottom topography and cannot be practically used. So, we generate the numerical grid which does not satisfy the criteria for the sigma-coordinate approach at any grid point exactly, but we still wish to employ this approach. The point resulting from this situation can be found in some deviation from the whole conception. As one of the approaches, we have evaluated the horizontal pressure gradient on the basis of the z-level coordinate system [16, 19]. The recent investigation by Kliem and Pietrzak [11] have shown that the

z-level-based approach is the simplest and effective to reduce the pressure gradient errors.

Remark. When working with a three-dimensional model using the separate mode approach, it is strongly recommended to use an integrated pressure gradient approximation in barotropic equations, the same as it was chosen for the baroclinic system. Otherwise, artificial circulation cells can occur in the picture of the volume transport function distribution.

2.2. Modeling of horizontal diffusion. On the time interval $0 < t < T$, we consider the diffusion transport processes of some substance T

$$\frac{\partial T}{\partial t} = \frac{\partial}{\partial x}\mu\frac{\partial T}{\partial x} + \frac{\partial}{\partial z}\nu\frac{\partial T}{\partial z}. \tag{5}$$

For the sake of simplicity the description is conducted in the section (x, z) of the ocean basin. Here: x is the horizontal coordinate, $x_0 < x < x_1$, z is the downward vertical coordinate increasing from the ocean surface $z = 0$ to the bottom topography $H(x)$; μ and ν are the horizontal and the vertical diffusion coefficients, respectively. If the coordinate system transformation (1) is used, our section of the ocean basin becomes a rectangle in the new coordinate system (x, σ), and then equation (5) will be the following:

$$H\frac{\partial T}{\partial t} = LT, \tag{6}$$

where

$$L = \frac{\partial}{\partial x}H\mu\frac{\partial}{\partial x} + \frac{\partial}{\partial \sigma}\frac{\nu}{H}\frac{\partial}{\partial \sigma} - \frac{\partial}{\partial x}\mu\sigma H_x\frac{\partial}{\partial \sigma} - \frac{\partial}{\partial \sigma}\mu\sigma H_x\frac{\partial}{\partial x} + \frac{\partial}{\partial \sigma}\mu\frac{\sigma^2 H_x^2}{H}\frac{\partial}{\partial \sigma}.$$

and $H_x = \frac{\partial H}{\partial x}$. The discrete analogue to equation (6) has been obtained through the use of the Finite Element Method (FEM) in which we employ linear basic functions. This method was the main technique used in our WOCM [3–5].

To obtain a numerical analogue, we set the regular grid x_i, σ_k with the grid spacing $\Delta x, \Delta\sigma$ on the rectangle section (x, σ) and denote it as Ω. Proceeding further, we make triangulation of a grid area Ω with diagonals in both positive and negative directions depending on the topography gradient (Figure 1). Let the unknown substance T be approximated as

$$T = \sum_{i,k\in\Omega} \omega_{ik} T_{ik}, \tag{7}$$

where ω_{ik} is piecewise linear, which is equal to 1 at a grid node (i, k) and to 0 at all others. The use of the Galerkin procedure for equation (6)

$$\int_\Omega H\frac{\partial T}{\partial t}\omega_{ik}d\Omega = \int_\Omega LT\omega_{ik}d\Omega \tag{8}$$

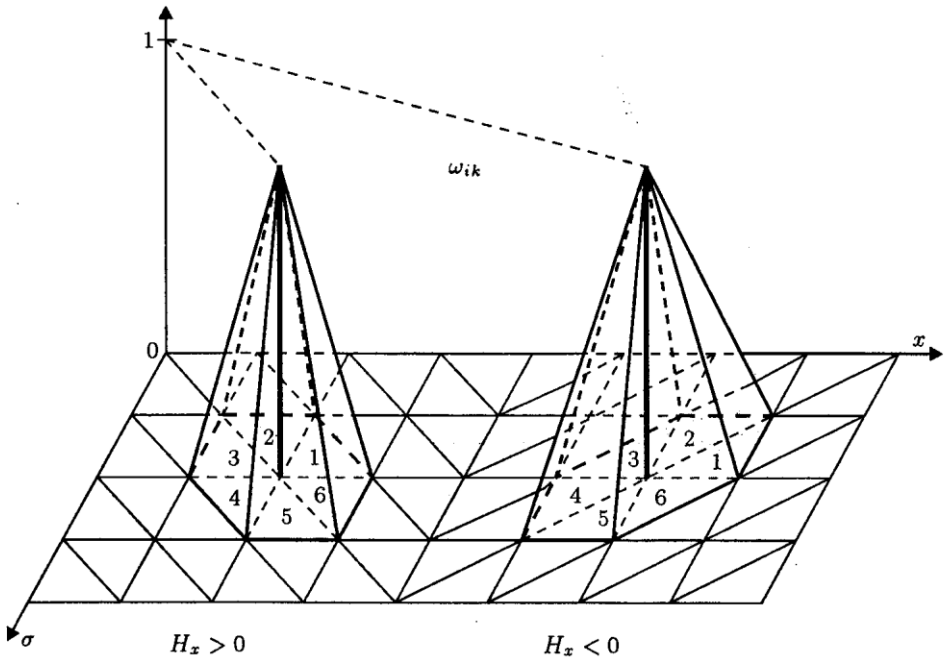

Figure 1. A numerical grid triangulation based on the topography gradient sign. The FEM basic functions. The numbers of triangles used in numerical scheme are ranged within 1 to 6

and substitution of approximation (7) yields a system of algebraic equations for the nodal points unknowns T_{ik}, which can be written in the matrix form:

$$M\frac{\partial T}{\partial t} = L_{xx}T + L_{\sigma\sigma}T + L_{x\sigma}T,$$

where M is the grid operator

$$MT = T_{ik}H_i \int_\Omega \omega_{ik} d\Omega,$$

and L_{xx}, $L_{\sigma\sigma}$, $L_{x\sigma}$ are one-dimensional operators in the horizontal direction, vertical direction, and the direction inclined at a positive or negative angle with the horizontal direction depending on a topography gradient:

$$\begin{aligned} L_{xx}T &= a_{i-1}T_{i-1,k} - (a_{i-1} + a_i)T_{ik} + a_iT_{i+1,k} \\ L_{\sigma\sigma}T &= b_{k-1}T_{i,k-1} - (b_{k-1} + b_k)T_{ik} + b_kT_{i,k+1} \end{aligned}$$

and $L_{x\sigma}$ depending on the grid triangulation. For deepening topography, when $H_{i+1} > H_i > H_{i-1}$

$$L_{x\sigma}T = c_{j-1}T_{i-1,k-1} - (c_{j-1} + c_j)T_{i.k} + c_jT_{i+1,k+1},$$

and when $H_{i+1} < H_i < H_{i-1}$

$$L_{x\sigma}T = c_{j-1}T_{i-1,k+1} - (c_{j-1} + c_j)T_{i,k} + c_jT_{i+1,k-1}.$$

In these expressions

$$a_i = \int_{\Delta_1 \cup \Delta_6} \frac{1}{\Delta x}\left(\frac{\mu H}{\Delta x} + \frac{\mu\sigma\,|H_x|}{\Delta\sigma}\right) d\Omega,$$

$$b_k = \int_{\Delta_5 \cup \Delta_4} \frac{1}{\Delta\sigma}\left(\frac{\nu}{H\Delta\sigma} + \mu\frac{\sigma^2 H_x^2}{H\Delta x}\right) d\Omega,$$

$$c_j = -\int_{\Delta_5 \cup \Delta_6} \frac{\mu\sigma\,|H_x|}{\Delta z\Delta x} d\Omega,$$

when $H_{i+1} > H_i > H_{i-1}$. Here $\Delta_1, \ldots, \Delta_6$ are the grid domain triangles as denoted in Figure 1. When the opposite triangulation is used (in the case of $H_{i+1} < H_i < H_{i-1}$), we have the same expression for the coefficients except for b_k which is calculated on the basis of the triangles $\Delta_5 \cup \Delta_6$ and c_k – on the basis of $\Delta_1 \cup \Delta_2$.

Following [20], we introduce the splitting algorithm to overcome the difficulties associated with solution of the two-dimensional problem

$$M\frac{T^*}{\Delta t} - L_{\sigma\sigma}T^* = M\frac{T^n}{\Delta t} + L_{\sigma\sigma}T^n + 2L_{xx}T^n + 2L_{x\sigma}T^n,$$

$$M\frac{T^{n+1}}{\Delta t} - L_{xx}T^{n+1} = M\frac{T^*}{\Delta t} - L_{xx}T^n.$$

We do not specify the boundary and the initial conditions here as they can be different, generally used for the description of the diffusion transport processes. Numerical tests were conducted for a simple diffusion problem in two-dimensional closed basin coinciding with a cross-section of the model ocean basin with real topography. To make sure about the possibility to apply the new method to an ocean problem, we took the meridional cross-section with a steep bottom slope and the same numerical grid (4.5° latitude and 21 vertical levels) as we were going to do with the WOCM. Initially, the isothermal basin with temperature $t = 0°C$ had a heat source $t = 25°C$ independent of latitude at the sea surface. Figure 2 represents 100 years of the numerical simulation for the horizontal diffusion coefficient later used in the climate model experiment (Section 3). The comparison was made for the same problem when using the approximation formula [13]. In contrast to the case of the approximation formula, the new approach enables obtaining quite a good isotherms distribution for the upper 1000 m layer. The isotherm 2°C has the most irregular behavior which can be a result not only of errors in the numerical algorithm, but a result of a long integration in the irregular region and the linear interpolation from the σ-levels. It should be noted that the approach described was an unexpected development of the previously

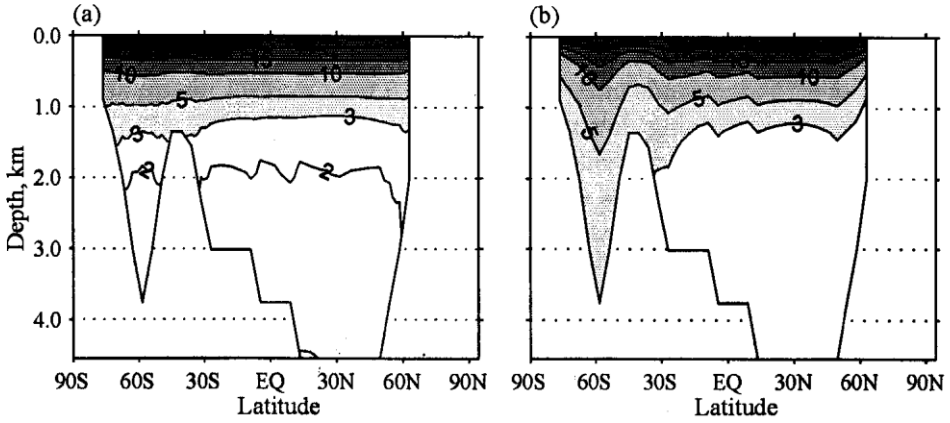

Figure 2. The temperature distribution in the diffusion transport test after 100 years-simulation using different approaches: (a) Goloubeva; (b) Mellor and Blumberg [13]

used method [15], employed in our World Ocean Model ([3–5]). In this method, the two-dimensional grid operator was split to a series of the three one-dimensional operators, each of them being positive semidefinite. In this case, for the condition $L_{x\sigma}$ to be positive semidefinite, the required grid triangulation should be in the opposite direction to that presented here and a strong restriction for the operator L_{xx} should be satisfied. As a result we can use either a very smoothed bottom topography or some multiplication coefficient less than 1 for the cross-derivative operator $L_{x\sigma}$. With the new triangulation described in this paper we strengthen the operator L_{xx} and obtain absolutely 'bad' $L_{x\sigma}$ for every grid node. The idea to put the 'bad' operator $L_{x\sigma}$ into the right-hand side of the split system made the problem solution successful. The new constraints on the topography gradient should be investigated. We have not done it in this work, just have convinced ourselves that the numerical test on the steepest gradient in the model topography gave an appropriate result.

3. The World Ocean Circulation modeling

The techniques described were incorporated into the three-dimensional World Ocean Circulation Model in the σ-coordinate system, which has been developed in the Laboratory of Oceanography of the Computing Center of the Siberian Branch of the Russian Academy of Sciences [3–5]. The control run was spun up to explore the possibility of using the sigma coordinate ocean model for the climatic investigation. Can this model reproduce the large-scale global oceanic dynamics without using any robust technique in the deep ocean? The model was applied to the global ocean basin restricted

to 73°N with approximate coastal boundary and a smoothed version of the real World Ocean bottom topography. A coarse horizontal mesh has a grid spacing of 3.75° longitude and 4.5° latitude. There were 21 unequally spaced vertical levels increasing downward.

The surface forcing was taken from the well-known climatological atlases. The model was forced at the sea surface by seasonally varying climatological boundary conditions of temperature, salinity, and wind stress. The surface monthly mean values were linearly interpolated to give daily forcing. The wind stress climatology used was that by Hellerman and Rosenstein [21]. Temperature and salinity are damping towards the climatological values by Levitus ([22, 23]) with uniform restoring time-scales of 30 days for temperature and 50 days for salinity. The specific feature of using this technique in the sigma-coordinate model is discussed in [16].

Values of model parameters are similar to those frequently used in the coarse resolution model studies. The horizontal (AMH) and the vertical (AMV) viscosity coefficients are taken to be constants independent of the depth (AMH = $2.5 \cdot 10^9$ cm^2/sec; AMV = 50 cm^2/sec). The vertical diffusion (AHV) is lowest in the surface layer (0.3 cm^2/sec), increasing below the thermocline (following Bryan and Lewis [24]) toward a maximum of 1.3 cm^2/sec in the deeper model levels. The horizontal diffusion AHH = 10^7 cm^2/sec in the surface level gradually decreases towards $0.5 \cdot 10^6$ cm^2/sec at the depths ([25]).

All the forcing data and grid configuration were chosen to maintain the consistency with the paper by M. England [25]. No deep accelerated time stepping was used during the experiment.

The model was starting from the ocean at rest with uniform thermohaline fields (2°C and 34.70 psu) independent of the depth. It took about 50 years of modeling to obtain the quasi-steady ocean circulation in the uppermost 500 m layer. The model was integrated over 1000 years more to obtain a relatively steady state for the deep ocean. Here we represent the annual-mean distribution of model characteristics at the end of numerical integration.

3.1. Horizontal circulation. Figure 3 shows the vertical integrated volume transport stream function. We just pay attention to the famous points of the picture. One can detect the established main subtropical circulation with some western intensification. Weak tropical and subpolar cell can be seen as well. The most intensive in the picture is the Antarctic Circumpolar Current. We should note that the coarse grid spacing could not permit us to obtain the realistic value of the velocity currents and their volume transport.

Starting from the subsurface upper oceanic layer (Figure 4a) the model results represent the main large-scale ocean currents in both hemispheres, such as the western boundary currents, the Equator Undercurrent and the

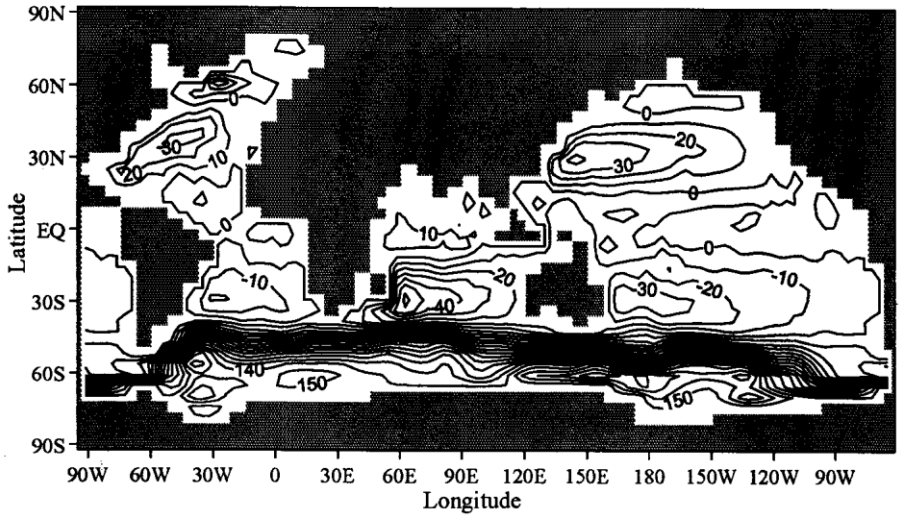

Figure 3. Horizontal stream function. Transport is shown in Sverdrups ($1\ \text{sv} = 10^{12}\ \text{cm}^3/\text{s}$)

Antarctic Circumpolar Current. Proceeding further, down to the intermediate layer we watch the disappearance of the well-established circulation structure. From 2000 down to 3000 m the model reproduces the west boundary flow from the North Atlantic to the South Atlantic (Figure 4b). This flow meets the ACC water at vicinity 45°S and turns to the east flowing further with ACC into the Indian ocean as an undercurrent to the Agulhas current in the West Indian Ocean. The bottom layers contribute basically to the meridional motion (Figure 4c). The circulation is represented with the northward flow from the Antarctic region to the three oceans and the southward flow in the eastern part of the South Atlantic and the Indian Ocean.

3.2. Meridional circulation. Figure 5 represents the meridional overturning circulation for different oceans. This pattern summarizes the main flow movement, which was already pointed out.

The global meridional circulation in the uppermost 500 m is mainly induced by the wind. Two shallow tropical cells represent the surface poleward Ekman transport for both hemispheres which is compensated by upwelling in the equatorial zone. In midlatitudes, the wind forcing intensifies the equatorward Ekman transport which, together with tropical poleward transport both generate the convergence zone in subtropics. Here the sinking branch is the part of the next circulation cell can be seen in each hemisphere. The cell in the Northern Hemisphere is very shallow and weak. On the contrary, the Southern Hemisphere has deep and strong Deacon cell between 60°S and 30°S, reaching 3000 m depth. Another counter-clockwise cell in the South

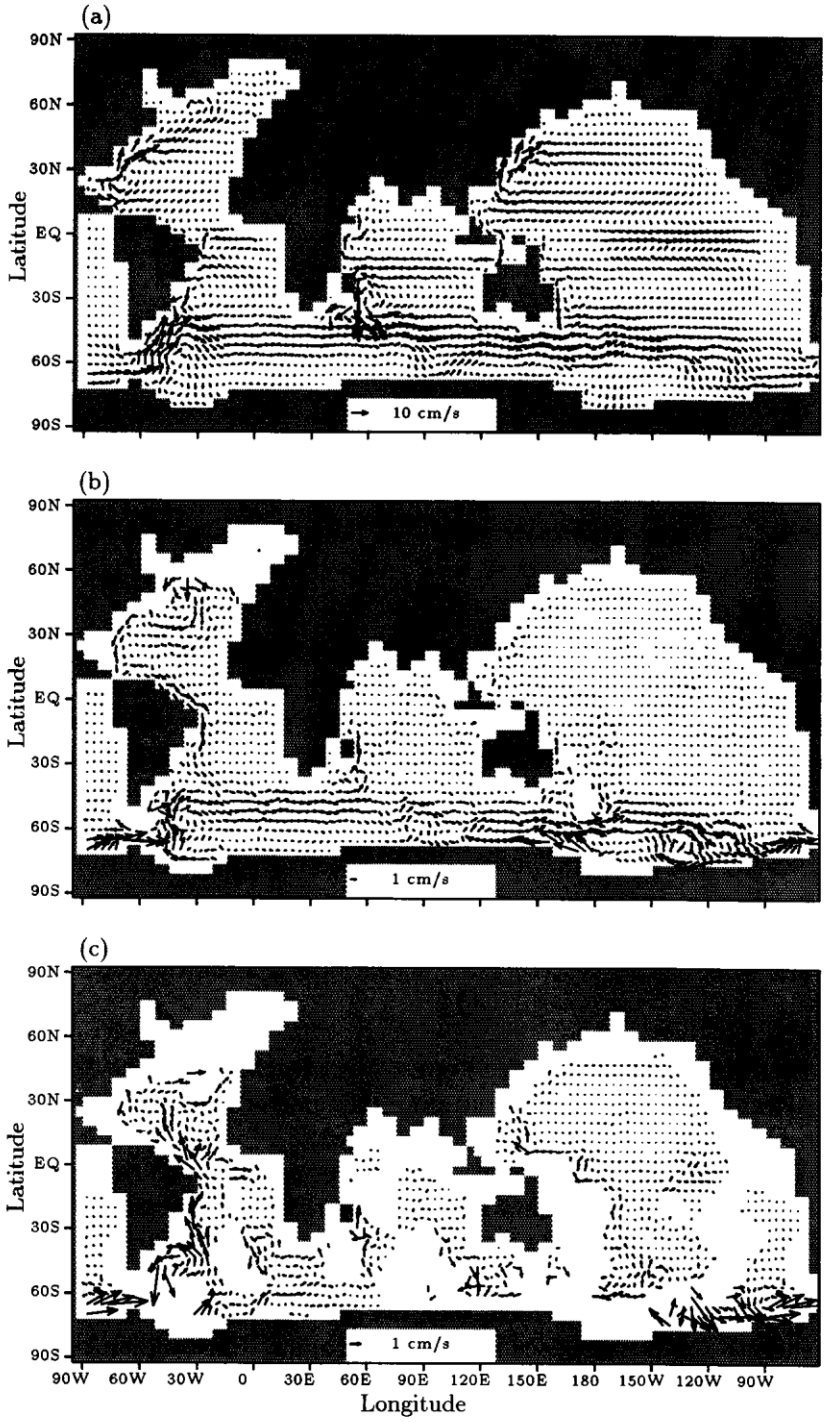

Figure 4. Flow fields simulated at depths (a) 185 m, (b) 2000 m, and (c) 4000 m

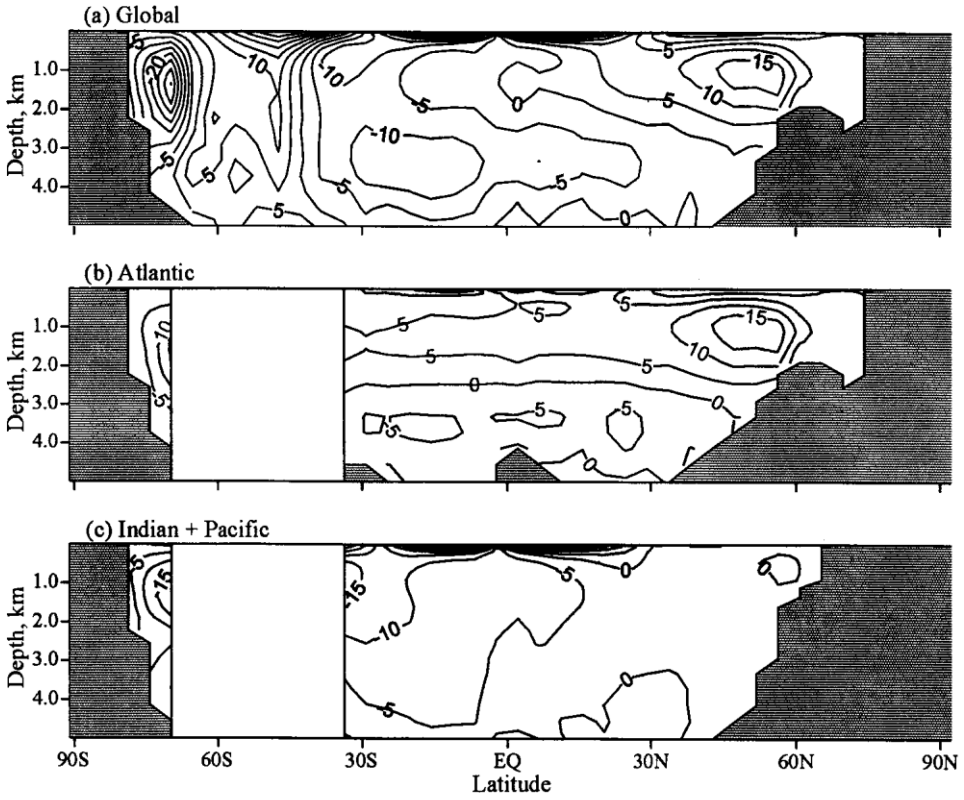

Figure 5. Meridional overturning stream function. Transport is shown in Sverdrups

Hemisphere is situated very close to Antarctida, where the deep convective sinking occurs.

The other features of the global meridional circulation can be better seen in the pictures for different ocean basins. The surface 1000 m layer in the Atlantic Ocean represents the northward water flow from the Southern Ocean that ends up with downwelling at 50–60°N. The closed circulation cell is typical of the North Atlantic. It represents a strong downwelling in the North Atlantic Bottom water formation zone and a slow upwelling in the Tropical Atlantic. The center of this cell is situated at about 1100 m depth in this model run. Down from this depth, the southward flow from the North Atlantic to the region of the Antarctic Circumpolar Current is denoted by horizontal isolines stretched from 60°N to 35°S. The opposite direction bottom flow, northward from the ACC zone is shown as three deep layer circulation cells. The circulation in the interior in the Indian Pacific basin is very different. The model distribution shows from 5 to 10 sv of the northward motion in the deep 2500 m layer. This circulation in cooperation with the Atlantic bottom layer current forms an intensive deep

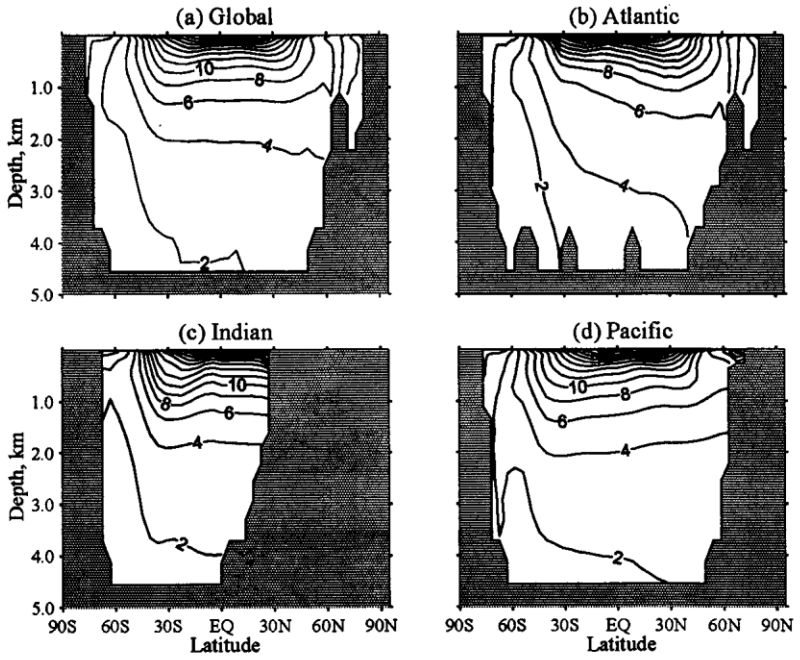

Figure 6. Zonal-mean potential temperature distributions. Results of the numerical modeling

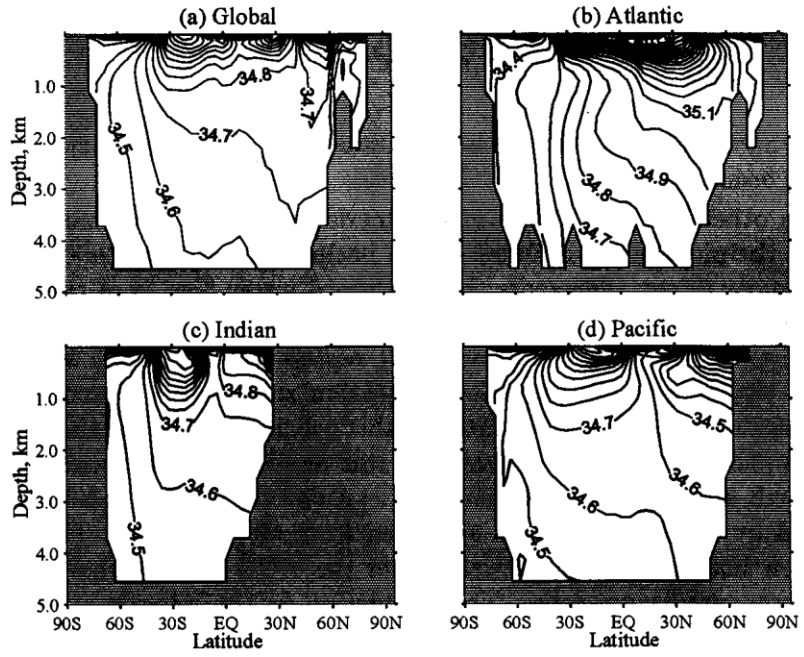

Figure 7. Zonal-mean salinity distributions. Results of the numerical modeling

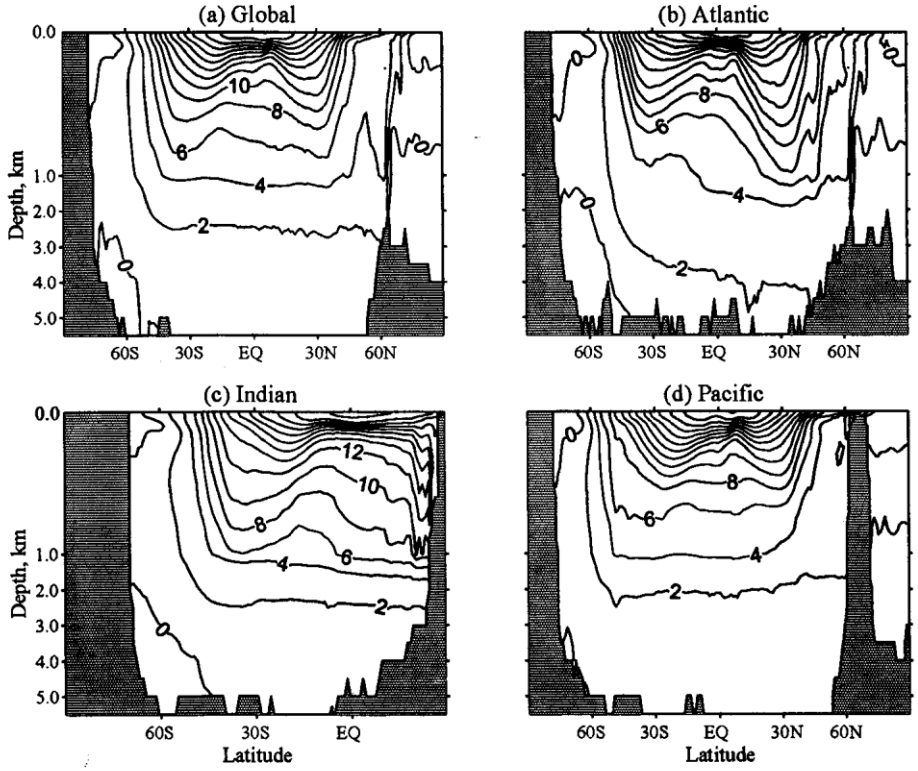

Figure 8. The observed annual and zonal-mean potential temperature climatology (Levitus, 1984)

layer circulation cell in the globally averaged picture. This cell is extending from the Antarctic Circumpolar Current boundary to the mid-latitude in the Northern Hemisphere. Without any discussion about shortcomings in the circulation presentation, we just say that this picture has a lot of similar features with the same numerical result obtained by the other modelers [25–27].

3.3. Thermohaline structure. Figures 6 and 7 represent the large-scale thermohaline structure in the model ocean. The picture pattern follows the global overturning processes, pointed out in Figure 5, and has similar features and problems as a lot of numerical climate results on the basis of coarse grids. To show the shortcomings of this model, we present the pictures of the observed climatology (Figures 8, 9). From a brief comparison between observational data and the model results we can distinguish the two main problems in our modeling: too warm deep layer in the model ocean and the lack of the Southern Hemisphere low-salinity tongues in the Indian and in the Pacific oceans.

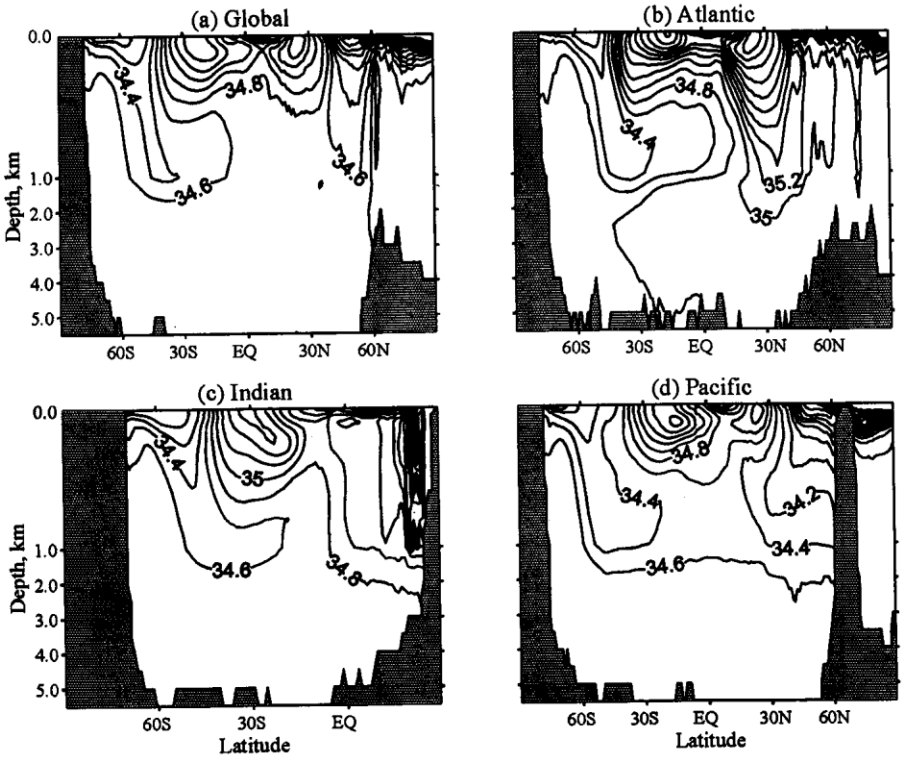

Figure 9. The observed annual and zonal-mean salinity climatology (Levitus, 1986)

4. Conclusion

Two main improvements concerning the pressure gradient approximation and the description of the diffusion processes were included into the World Ocean Circulation Model employed in the sigma coordinate system. It has been shown, using a coarse grid model run for 1000 years integration period, that important properties of the observed global large-scale thermohaline circulation could be reproduced on the basis of the sigma coordinate approach within the restrictions imposed by grid spacing and physical filling of the numerical model. It is worth while to mention that in th is experiment we did not try to use the advantages of the sigma-coordinate approach, but just explore the general possibilities to work with this approach with the steep bottom topography for a long integration period. A number of numerical and physical improvements should be made for the model to reproduce a reliable climate distribution. The inclusion of the Arctic Ocean and sea ice, real-flux condition at the sea surface, higher-order numerical scheme for the advective transport, isopicnic parameterization of turbulent mixing and the diffusion of all of these items can be the subject of future investigations.

Acknowledgements. I wish to thank Dr. Matthew England who initiated this work. He generously provided all the climate data and grid arrays and gave me a lot of very helpful suggestions and comments during my work in Australia at the University of New South Wales.

References

[1] Blumberg A.F., Mellor G.L., A description of three-dimensional coastal ocean circulation model // Three Dimensional Coastal Ocean Models, Coastal Estuarine Sci. Ser. – Washington D.C.: AGU, 1987. – Vol. 4. – P. 1–16.

[2] Haidvogel D.B., Wilkin J.L., Young R.E. A semi-spectral primitive equation ocean circulation model using vertical sigma and orthogonal curvilinear horizontal co-ordinates // J. Comput. Phys. – 1991. – Vol. 94. – P. 151–185.

[3] Kuzin V.I. The Finite Element Method in the Ocean Processes Modeling. – Novosibirsk: Computing Center, 1985 (in Russian).

[4] Goloubeva E.N. Numerical Modeling of the Middle-Term Climatic and Seasonal Circulation of the World Ocean: Ph.D. thesis. – Novosibirsk: Computing Center, 1989 (in Russian).

[5] Goloubeva E.N., Ivanov Ju.A, Kuzin V.I., Platov G.A. Numerical modeling of the World Ocean circulation including upper ocean mixed layer // Oceanology. – 1992. – Vol. 32, № 3. – P. 395–405 (in Russian).

[6] Marchuk G.I., Dymnikov V.P., Zalesnyj V.B. Mathematical Models in Geophysical Hydrodynamics and the Numerical Methods of Their Implementation. – Leningrad: Gidrometeoizdat, 1987 (in Russian).

[7] Moshonkin S.N., Semenov E.V., Zalesny V.B. Circulation of the World ocean: the effect of physical factors on the formation and the long-term variability of hydrophysical fields // Russ. J. Numer. Anal. Math. Model. – 1998. – Vol. 13, № 6. – P. 517–536.

[8] Zalesny V.B., Moshonkin S.N. Equilibrium thermohaline regime of model global ocean circulation // Izvestija, Atmospheric and Ocean Physics. – 1999. – Vol. 35, № 3. – P. 371–398 (in Russian).

[9] Haney R.L. On the pressure gradient force over steep topography in sigma coordinate ocean models // J. Phys. Oceanogr. – 1991. – Vol. 21. – P. 610–619.

[10] Beckmann A., Haidvogel D.B. Numerical simulation around a tall isolated sea mount. Part 1. Problem formulation and model accuracy // J. Phys. Oceanogr. – 1993. – Vol. 23. – P. 1736–1753.

[11] Kliem N., Pietrzak J. On the pressure gradient error in sigma coordinate ocean models: A comparison with a laboratory experiment // J. Geophys. Res. – 1999. – Vol. 104, № C12. – P. 29781–29799.

[12] Song Y.T., Wright D.G. Ageneral pressure gradient formulation for ocean models. Part 2: Energy, momentum, and bottom torque consistency // Mon. Weather Rev. – 1998. – Vol. 126. – P. 3231–3247.

[13] Mellor G.L., Blumberg A.F. Modelling vertical and horizontal diffusivities and the sigma co-ordinate system // Mon. Weather Rev. – 1985. – Vol. 113. – P. 1379–1383.

[14] Huang W., Spaulding M. Modeling horizontal diffusion with sigma coordinate system // J. Hydravlic Eng. – 1996. – P. 349–352.

[15] Marchuk G.I., Kuzin V.I. On combination of finite element and splitting-up method of parabolic equations // J. Comp. Phys. – 1983. – Vol. 52, № 2. – P. 237–272.

[16] Goloubeva E.N., England M.H. Intercomparison of Global Ocean Circulation Models (to appear).

[17] Phillips N.A. A co-ordinate system having some special advantages for numerical forecasting // J. Meteorol. – 1957. – Vol. 14. – P. 184–185.

[18] Mesinger F. On the convergence and errors problems of the calculation of the pressure gradient force in sigma co-ordinate models // Geophys. Astrophys. Fluid Dyn. – 1982. – Vol. 19. – P. 105–117.

[19] Platov G.A., Middleton J.F.F. Notes on pressure gradient correction // This issue.

[20] McKee S., Mitchel A.R. Alternating direction methods for parabolic equations in two space dimensions with a mixed derivative // The Computer Journal. – 1970. – Vol. 13, № 1.

[21] Hellerman S., Rosenstein M. Normal monthly wind stress over the World Ocean with error estimates // J. Phys. Oceanogr. – 1983. – Vol. 13. – P. 1093–1104.

[22] Levitus S. Annual cycle of temperature and heat storage in the World Ocean // J. Phys. Oceanogr. – 1984. – Vol. 14. – P. 727–746.

[23] Levitus S. Annual cycle of salinity and salt storage in the World Ocean // J. Phys. Oceanogr. – 1986. – Vol. 16. – P. 322–343.

[24] Bryan K., Lewis L.J. A water mass model of the World Ocean // J. Geophys. Res. – 1997. – Vol. 85. – P. 2503–2517.

[25] England M. Representing the global scale water masses in general circulation models //J. Phys. Oceanogr. – 1993. – Vol. 23. – P. 1523–1550.

[26] Manabe S., Stouffer R.J. Multiple-century response of a coupled ocean-atmosphere model to an increase of atmospheric carbon dioxide // J. Climate. – 1994. – Vol. 7. – P. 5–23.

[27] Jiang S., Stone P., Malanotte-Rizzoli P. An assessment of the geophysical fluid dynamics laboratory ocean model with coarse resolution: annual-mean climatology // J. Geophys. Res. – 1999. – Vol. 104, № C11. – P. 25623–25645.